EUROPHYSICS LETTERS 15 October 2001

Europhys. Lett., **56** (2), pp. 221–227 (2001)

Parity breaking in a one-dimensional pattern: A quantitative study with controlled wavelength

P. Brunet, J.-M. Flesselles and L. Limat

Laboratoire PMMH-ESPCI - 10 rue Vauquelin, 75005 Paris, France

(received 29 January 2001; accepted in final form 23 July 2001)

PACS. 47.20.Lz – Secondary instability.
PACS. 47.54.+r – Pattern selection; pattern formation.

Abstract. – We have quantitatively investigated the parity-breaking bifurcation in a liquid column pattern with periodic boundary conditions formed below an overflowing dish. For high enough viscosity homogeneous global drifting states can be stabilized within a large range of wavelengths. Data are analyzed in terms of coupled phase and amplitude equations and show that the bifurcation to a global drifting state is supercritical, the flow rate and phase gradient behaving as effective control parameters. The wavelength dependence shows that new non-linearities must be added to the usual model. We also identify at large flow rate a regime of spatio-temporal chaos that mixes oscillations, drifts, coalescences and nucleations of columns.

Previous works and knowledge on parity-breaking bifurcation. – One-dimensional patterns formed by instabilities have been studied in many experiments [1–9]. Within generic behaviors associated to secondary bifurcations [10], parity breaking is most often observed: asymmetrical, dilated cells drift at constant speed $V_{\rm d}$ inside domains whose boundaries drift in the opposite direction. It was first observed by Simon *et al.* [1] on isotropic/nematic fronts in liquid crystals and later in various systems, such as Rayleigh-Benard convection [2], directional solidification fronts [6,7], viscous fingering between rotating cylinders (printer's instability) [4,5], and more recently the overflowing fountain [8,9]. The propagation of these drifting domains is a major mechanism of wavelength selection [7]. In addition, they are presumably directly involved in the genesis of spatio-temporal chaos. Hence, understanding the laws governing the bifurcation to these broken-parity states would shed an essential light on the physics on one-dimensional cellular patterns. Two related models are found in the literature that describe at least qualitatively this bifurcation. The first one [11] invokes non-linear interactions between a basic mode k_0 and its first harmonic $2k_0$ (this is often called a "q-$2q$" model), the drift being a consequence of a phase shift occuring between these two modes. The second one [12] (often called "C3G" model after the author's initials) adds an antisymmetrical perturbation $U_{\rm A}(k_0x) = -U_{\rm A}(-k_0x)$ to a basic symmetrical state $U_{\rm S}(k_0x) = U_{\rm S}(-k_0x)$, so that a typical field representative of the pattern structure (fluid velocity, interface position) reads

$$U(x,t) = U_{\rm S}(k_0x + \phi(x,t)) + A(x,t)U_{\rm A}(k_0x + \phi(x,t))\,, \qquad (1)$$

where x is the space coordinate, t the time, $\phi(x,t)$ the spatial phase of the pattern and $A(x,t)$ the amplitude of perturbation. The quantities $A(x,t)$ and $\phi(x,t)$ are coupled by non-linear equations deduced from symmetry arguments [10, 12], that at lowest order read

$$A_t = (\mu + \epsilon\phi_x)A + A_{xx} + \gamma A A_x - \delta A^3 + \dots , \tag{2}$$

$$\phi_t = \omega A + \phi_{xx} + \dots , \tag{3}$$

where μ is the control parameter, ϵ, ω and δ are coefficients. This minimal model has been completed by adding other terms [13], but most of these vanish in the bulk of drifting domains. It is expected to capture most of the physics at least near threshold.

Within such a model, sufficiently dilated cells ($\mu + \epsilon\phi_x > 0$) drift through the ωA term. In the initial model, the bifurcation towards a drifting state was assumed to be subcritical ($\delta < 0$), in order to have coexisting static and drifting domains. But as shown in more recent advances [13], the supercritical case ($\delta > 0$) is well adapted to explain most of the observed phenomenology. Assuming that A and ϕ_x are constant inside a drifting domain, the velocity of the cells is then simply given by [7]

$$\phi_t = kV_{\mathrm{d}} = \frac{\omega}{\delta^{1/2}}(\mu + \epsilon\phi_x)^{1/2} , \tag{4}$$

where $k = 2\pi/\lambda$ is the wave number inside the drifting domains, and $\phi_x = k - k_0$ is the wave number mismatch between the drifting and the reference states. Although these ideas are now well established, the agreement between theory and experiment is only qualitative. Few experiments have quantitatively investigated the relevance of these models and tried to check directly eq. (4) or its equivalents. To our knowledge, the only quantitative available study has been performed by Pan and de Bruyn [5] for the printer's instability. The data were in good agreement with eq. (4) after replacing μ with a linear function of the rotation velocities of the cylinders. The generality of these results remains, however, to be established for other systems. In addition, since the $\epsilon\phi_x$ term was negligible in their system, their test of the theory was incomplete. Therefore, an experimental investigation including the wavelength dependence remains to be done.

The fountain: aim of the present study. – The pattern of liquid columns reproduced in fig. 1a is well adaptated to such a study. These columns are formed when a liquid arrives at a constant rate at the center of a circular overflowing dish and falls from its perimeter. A previous study [8] has revealed that a global uniform drift of this pattern can be forced with different numbers of columns (N).

In [8], the range of wavelength was rather restricted. Here, we continue the exploration of the pattern dynamics, but for a higher viscosity ($\eta = 100\,\mathrm{cP}$). We observe an increase in the range of the drifting states stability. For a given value of the flow rate, this allows us to study up to 14 (varying also the dish diameter) different wavelengths in the global drift regime (a range of 0.6 cm for a central value of 1.8 cm) and thus to perform the quantitative study suggested above. Global drift states are also compared to local drifts. In this last situation, the system itself selects the wavelengths inside and outside the domains [9]. However, it is found that the same laws govern both situations.

Experimental setup. – Silicon oil of viscosity $\eta = 100\,\mathrm{cP}$, surface tension $\gamma = 20$ dynes/cm and density $\rho = 0.97\ \mathrm{g/cm^3}$ at $20\,^{\circ}\mathrm{C}$ is injected at the dish center through a hollow vertical tube. The flow is measured by a float flowmeter (Brooks Full View GT 1024) and kept constant by a gear pump (Ismatec BVP Z) followed by a cylindrical damping chamber (half-filled) (radius = 20 cm, height = 15 cm). The imposed flow rate Q ranges from 2 to $30\,\mathrm{cm^3/s}$.

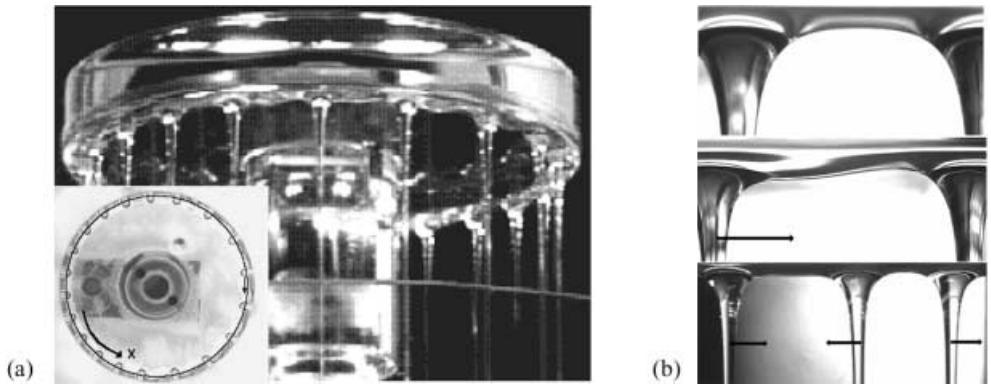

Fig. 1 – (a) Side and top view of a liquid column array formed below an overflowing transparent circular dish. The liquid is injected at the center of the dish through the vertical central tube. Columns are lighten by a circular neon tube surrounding the dish and placed underneath (insert: view from above). (b) Closer side views of interfaces. From top to bottom: static, drifting and oscillating columns (arrows indicate motion). Horizontal sizes of pictures are, respectively, 1.1 cm, 2 cm and 3.1 cm.

The oil temperature is regulated with a thermal bath at 20 °C with a few percent accuracy. Plexyglass circular dishes with different geometrical features have been used, but only the external radius R_e was found to be the only relevant parameter through the flow rate per unit length $\Gamma = Q/2\pi R_e$. The data reported here were obtained with two dishes of radii $R_e = 5$ cm and 8.35 cm. The accuracy of the dish horizontality is crucial for a quantitative study. In our previous works it was checked by using the deflection of a laser beam reflected by the liquid surface (accuracy 0.02°). In the course of our study, we found that an even better accuracy was obtained by simply checking the uniformity of oscillation amplitudes of columns when the system undergoes a transition to an oscillatory state (see below, "Osc" regime).

As usual, these dynamical regimes are visualized by means of spatio-temporal diagrams. Observed from above by a video camera, and lighten by a circular neon tube, the pattern appears as a series of circles (see insert in fig. 1a). The spatio-temporal diagrams are built by recording grey levels along the circle on which the column centers are moving. Experimentally this radius was found to be independent of the flow rate and respectively equal to $R = 4.77$ cm and $R = 8.10$ cm for the dishes of radius $R_e = 5$ cm and $R_e = 8.35$ cm.

Exploration of phase space by varying initial conditions. – When the flow rate is progressively increased, starting from zero, the pattern of liquid columns replaces a dripping state just above $\Gamma \simeq 0.05\,\mathrm{cm^2\,s^{-1}}$. With the 100 cP oil used here, one gets a static pattern of wavelength of order $1.05\,\mathrm{cm} \pm 0.1\,\mathrm{cm}$. This value can be modified with thin needles put in capillary contact with the top part of one or two columns. Once the columns follow the needle [8], one can force coalescence of neighboring columns, or nucleation of a new column by taking two columns apart enough. One can also induce larger strains of the pattern by moving a column at a constant speed during a long enough time. The needle induces successive coalescences of the forward neighbors it crosses while the motion is communicated to the backward neighbors. This method was previously used to induce a global drift of the pattern or to generate localized drifting domains [8]. More generally, it allows us to control the initial conditions: number N of cells, their position and speed. By combining these two methods, one can explore a "phase space" (see fig. 3a below) built upon the flow rate per unit length Γ and the mean wavelength

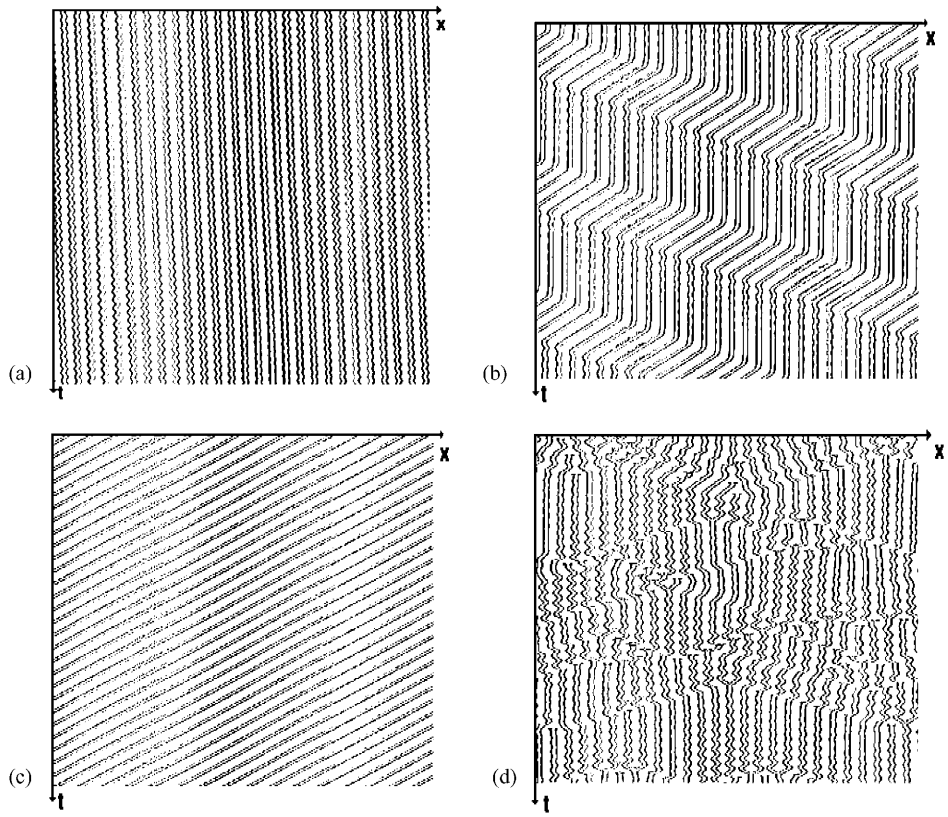

Fig. 2 – Different dynamical regimes visualized by spatio-temporal diagrams (their duration is typically 30 s). The horizontal axis represents the circle intercepting column centers, whose perimeter is equal to 30.2 cm. The left and right parts of this axis are connected due to periodic boundary conditions. (a) Oscillations with spatial period doubling (Osc), (b) propagation of localized drifting domains (LD), (c) global drift of the whole pattern (GD), (d) spatio-temporal intermittency (STI).

$\lambda_m = 2\pi R/N$. Depending on these two parameters, one observes different states on the liquid column array. In a rather narrow band of wavelength the static pattern is stable; the liquid arches connecting two columns are symmetrical (fig. 1b, top part). Above a value of order 1.10 cm, *i.e.* for a sufficiently elongated pattern, transitions to dynamical states are observed. A sample of the obtained diagrams is displayed in figs. 2, the stability domain of each of these states being reproduced in fig. 3a.

Regimes close to onset: oscillations and local drifts. – For λ_m slightly larger than 1.10 cm, an oscillatory regime (Osc) is observed, exhibiting a spatial period doubling (fig. 2a). The position of each column oscillates, this oscillation remaining out of phase with that of the two nearest neighbors. The liquid arches remain symmetrical (fig. 1b, bottom part). A further increase of λ_m leads to a local drift regime (LD), in which localized broken-parity domains (asymmetrical liquid arches as in fig. 1b, middle part) are travelling along the dish perimeter (fig. 2b). The drifting domain is followed by transient oscillations (a behaviour also observed in numerical simulations [14]) the duration of which is increasing with flow rate. The wavelength selected outside the drifting domains is independent of the flow rate and its value ($\lambda_0 = 1.07$ cm) is close to the threshold of 1.10 cm mentioned above.

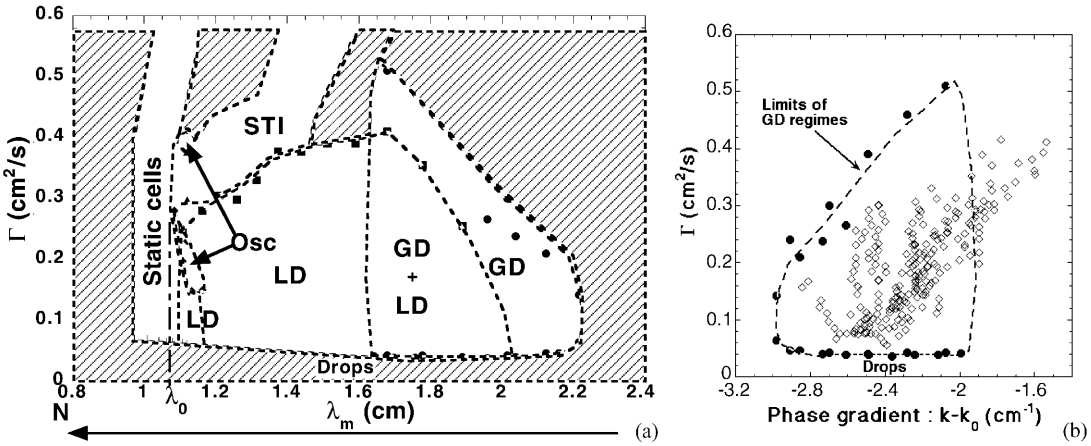

Fig. 3 – (a) Dynamical states existing for given values of flow rate Γ and mean wavelength λ_{m}; SC: static cells, Osc: oscillations, LD: localized drifting domains, GD: global drift, STI: spatio-temporal intermittency. Beyond the upper limit ($\Gamma = 0.57\,\mathrm{cm}^2/\mathrm{s}$), a liquid sheet is created. The hatched regions mean that no stationary state exists for such conditions. (b) Stability of drifting states: allowed phase gradient for a given flow rate. Circles and dashed line represent the limit of global drifts, diamonds represent measurements on localized drifting domains.

Regimes far from onset: global homogeneous drifts. – For large enough λ_{m}, the drifting domain can fill the whole dish perimeter (fig. 2c). We call this a global drifting state (GD in fig. 3a). With appropriate choices of the needle velocity, we are able to force such a state with different wavelengths λ. The range of allowed values appears in fig. 3a. In the best conditions ($\Gamma \simeq 0.1\,\mathrm{cm}^2\,s^{-1}$), λ can vary between 1.65 cm and 2.2 cm. With the two dishes, we explored fourteen values of λ, an improvement compared to the previous study [8] where at most three values of λ were investigated. In fig. 3b, we have plotted the range of allowed phase gradients $k - k_0$ ($k = 2\pi/\lambda$) *vs.* the flow rate. The range of values is less extended in local drifts than in global drifts (the system is then more constrained). This is another quantitative advantage of global drift study.

Mixed regimes and chaos. – In addition to these well-known states, we have discovered a regime of spatio-temporal intermittency (STI) at high flow rates (see fig. 2d) where oscillations, drifts, column nucleations and coalescences are combined in a complicated way, which results in a permanent irregular motion. Contrary to previous experiments [15], the absence of edge effects is an advantage for future investigations of the transition towards spatio-temporal chaos.

Quantitative study of drifting regimes. – We now focus on the quantitative study of the parity-breaking bifurcation. When plotted *vs.* the flow rate, for different wavelengths, the reduced drift velocity of a globally drifting pattern kV_{d} involved in eq. (4) behaves as $(\phi_t)^2 = (V_{\mathrm{d}}k)^2 = a(\phi_x)(\Gamma - \Gamma_0(\phi_x))$, where $a(\phi_x)$ and $\Gamma_0(\phi_x)$ are functions of the phase gradient ϕ_x (see fig. 4a). This phase gradient will now be defined with respect to the "ideal" state of wavelength λ_0 left behind a localized domain $\phi_x = k - k_0 = 2\pi(1/\lambda - 1/\lambda_0)$. As appears in fig. 4b, $\Gamma_0(\phi_x)$ is a linear function of the phase gradient. This fact, combined with the linear dependence of $(V_{\mathrm{d}}k)^2$ upon Γ, is in favour of a supercritical bifurcation governed by eq. (4), the reduced control parameter being equal to $\mu = (\Gamma - \Gamma_{\mathrm{c}})/\Gamma_{\mathrm{c}}$, with $\Gamma_{\mathrm{c}} = 0.0415\,\mathrm{cm}^2/\mathrm{s}$.

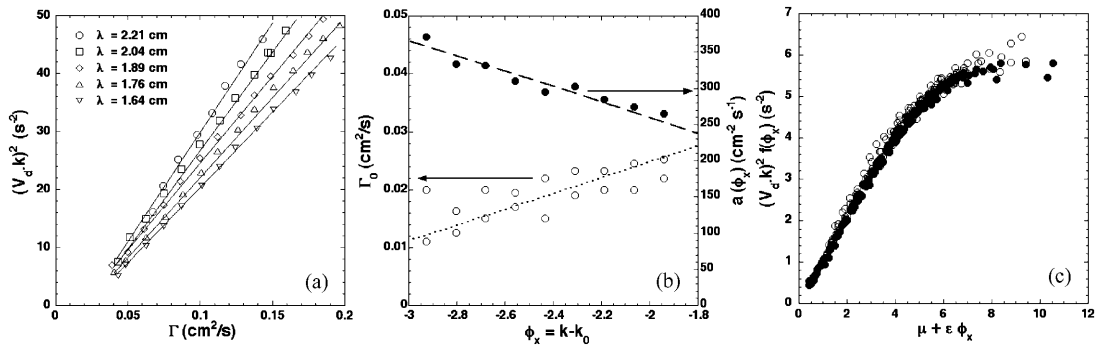

Fig. 4 – (a) Square of $k \cdot V_\mathrm{d}$ *vs.* Γ for different wavelengths. (b) Threshold ($\Gamma_0(\phi_x)$, open circles) and slope ($a(\phi_x) = \frac{\Delta(V_\mathrm{d} \cdot k)^2}{\Delta\Gamma}$, closed circles) extracted from the previous graphic, *vs.* phase gradient. (c) Rescaling of the whole set of data on a single master curve of equation $k^2 {V_\mathrm{d}}^2 f(\phi_x) = (\mu + \epsilon\phi_x)$ with $\mu = (\Gamma - \Gamma_\mathrm{c})/\Gamma_\mathrm{c}$, $\phi_x = k - k_0$ and $f(\phi_x) = g_2(\phi_x)/g_3(\phi_x)^2$. Black symbols: global drifts with fourteen different values of λ. Open symbols: measurements performed on local drifting domains.

The surprise here is however that the slope $a(\phi_x)$ is not constant, even close to threshold as appears in fig. 4b, and is a linear function of ϕ_x too. This imposes to reconsider the minimal model of eqs. (2)-(3), to which we have to add higher-order non-linearities. To be consistent with the initial idea of this model, we have kept most of the lowest-order terms allowed by symmetries.

Considering that A and ϕ_x are constant in the bulk of drifting domains, the most general form of the model reads

$$A_t = (\mu + g_1(\phi_x))A - g_2(\phi_x)A^3 + \dots , \tag{5}$$

$$\phi_t = g_3(\phi_x)A + \dots , \tag{6}$$

where g_1, g_2 and g_3 are polynomial functions. This extension is partly motivated by the fact that ϕ_x varies in a large range (fig. 3b). Equation (4) is then replaced by

$$\phi_t^2 = (kV_\mathrm{d})^2 = (\mu + g_1(\phi_x))\frac{g_3(\phi_x)^2}{g_2(\phi_x)} , \tag{7}$$

$\mu + g_1(\phi_x)$ being the effective control parameter of the bifurcation. According to fig. 4b, g_1 is equal to $\epsilon\phi_x$ and the ratio $\frac{(g_3)^2}{g_2}$, representing the slope $a(\phi_x)$, has to be linear with ϕ_x: this impose g_2 to be ϕ_x-dependent. The simplest solution is $g_2 = (1 + \beta\phi_x)$ and $g_3 = \nu(1 + \beta\phi_x)$, with $\nu = 1.77\,\mathrm{s}^{-1}$, $\beta = -1.25\,\mathrm{cm}$ and $\epsilon = 0.217\,\mathrm{cm}$.

Defining $f(\phi_x) = \frac{1}{a(\phi_x)} = g_2(\phi_x)/g_3(\phi_x)^2 = \frac{1}{\nu^2}(1 + \beta\phi_x)^{-1}$, we have plotted the quantity $f(\phi_x)(V_\mathrm{d} \cdot k)^2$ in fig. 4c, providing a nearly perfect fit of the whole set of data. On the same graph, we have also plotted measurements performed on local drifting domains (k and k_0 being respectively measured inside and outside the domain). Considering the non-trivial mechanism of wavelength selection, the lining tendency of this new set of points on the master curve is striking, and suggests that our empirical law is a fundamental feature of this system. This graph also confirms that the dynamics of local and global propagative domains are governed by the same laws, concerning the relationships between their speed, dilation and flow rate, the last two constituting an effective control parameter for a supercritical bifurcation. We were not able to justify the fact that the same coefficient β appears in eqs. (8) and (9) and

we conjecture that a hidden symmetry remains to be identified. Anyway, these ideas suggest to replace the initial version of the model by these equations

$$A_t = (\mu + \epsilon\phi_x)A + \gamma A_x A + A_{xx} - (1 + \beta\phi_x)A^3 + \dots, \tag{8}$$

$$\phi_t = \nu(1 + \beta\phi_x)A + D_\phi\phi_{xx} + \dots. \tag{9}$$

Other terms combining space and time derivatives of A and ϕ are allowed by symmetries and can be found in Caroli *et al.* [13]. The $A\phi_x$ term in eq. (9) was already included in this reference but the $A^3\phi_x$ one in eq. (8) is new. To our knowledge, our study is the first which puts into evidence the necessity to combine these factors and to measure with accuracy the coefficients of the C_3G model.

Conclusion. – These data allow us to draw the following conclusions. The C3G model (reconsidered with a supercritical global bifurcation) fails to account for the wavelength dependence in broken-parity states, even near threshold. An adequate description requires to take into account additional non-linearities that couple the phase gradient to the amplitude of the broken-parity component of the pattern, both near and far from threshold. Our experiment makes it clear and it presumably holds for all one-dimensional patterns. Finally, an additional qualitative result of our study is also the existence at high viscosity of a spatio-temporal chaos regime in the liquid column array. Again, the circular geometry will allow accurate studies without bias introduced by boundaries.

REFERENCES

[1] Simon A., Bechhoefer J. and Libchaber A., *Phys. Rev. Lett.*, **61** (1988) 2574.
[2] Daviaud F., Dubois M. and Bergé P., *Europhys. Lett.*, **9** (1989) 441.
[3] Flesselles J.-M., Simon A. J. and Libchaber A. J., *Adv. Phys.*, **1** (1991) 40.
[4] Michalland S., Rabaud M. and Couder Y., *Europhys. Lett.*, **22** (1993) 17.
[5] Pan L. and de Bruyn J. R., *Phys. Rev. E*, **49** (1994) 483.
[6] Ginibre M., Akamatsu S. and Faivre G., *Phys. Rev. E*, **56** (1997) 780.
[7] Faivre G. and Mergy J., *Phys. Rev. A*, **46** (1992) 963.
[8] Counillon C., Daudet L., Podgorski T., Jullien M.-C., Akamatsu S. and Limat L., *Europhys. Lett.*, **40** (1997) 2117.
[9] Brunet P., Flesselles J.-M. and Limat L., *Compte-rendus de la 3ème Rencontre du Non-Linéaire* (Edition Université de Paris Sud) 2000, pp. 203–208.
[10] Coullet P. and Iooss G., *Phys. Rev. Lett.*, **64** (1990) 866.
[11] Fauve S., Douady S. and Thual O., *J. Phys. (Paris)*, **1** (1991) 311.
[12] Goldstein R. E., Gunaratne G. H., Gil L. and Coullet P., *Phys. Rev. A*, **43** (1991) 6700.
[13] Caroli B., Caroli C. and Fauve S., *J. Phys. I*, **2** (1992) 281.
[14] Gil L., *Europhys. Lett.*, **48** (1999) 156.
[15] Rabaud M., Michalland S. and Couder Y., *Phys. Rev. Lett.*, **64** (1990) 184